Korean J. Chem. Eng., 40(8), 1892-1900 (2023)
DOI: 10.1007/s11814-023-1511-2

pISSN: 0256-1115
eISSN: 1975-7220

Reusable Pd nanoparticle catalysts supported on KOH-activated waste coffee grounds for the catalytic reduction of 4-nitrophenol

Hyeonjeong Ryu*, Eunhae Park*, Rengaraj Selvaraj,†, and Younghun Kim*,†**

*Department of Chemical Engineering, Kwangwoon University, Wolgye-dong, Nowon-gu, Seoul 01897, Korea
**Department of Chemistry, College of Science, Sultan Qaboos University, Muscat, Oman
(*Received 19 March 2023 • Revised 4 June 2023 • Accepted 9 June 2023*)

Abstract−Waste coffee grounds (CGs) are typically incinerated or sent to landfills, which can pollute the environment. However, after chemical treatments, such as carbonization and KOH-activation, CGs can exhibit macroporous and microporous structures, besides high chemical stability and surface area (2,710 m^2/g). Thus, activated CGs (ACGs) may be used as catalyst supports. Herein, Pd nanoparticles (NPs) loaded with ACG catalysts were prepared by two different methods: immobilization of PdNPs on the support and in situ reduction of Pd ions to Pd metal in the support. The catalytic performance of the ACG-supported PdNPs for the reduction of 4-nitrophenol to 4-aminophenol was investigated. In the recycling test, the ACG-supported PdNP catalysts outperformed the unsupported PdNPs in terms of the stability and conversion efficiency. Thus, the as-prepared ACG support was determined to be a suitable candidate for aqueous catalytic reactions.

Keywords: Waste Coffee Ground, Palladium Nanoparticles, 4-Nitrophenol, 4-Aminophenol, Catalytic Reduction

INTRODUCTION

Millions of people consume coffee daily, making it one of the most popular beverages worldwide [1]. Over time, the amount of waste coffee grounds (CGs) has increased in tandem with the amount of coffee consumed [2]. Waste CGs are typically treated as solid waste, which pollutes the environment through landfill or incineration. To reduce the amount of waste CG, research is being conducted on recycling or upcycling spent CGs into compost, building materials, and adsorbents [3-5]. Waste CG is a porous organic material with a high carbon content, large specific surface area, and easily controllable functional groups. In addition, activated carbon (AC) can be prepared from waste CGs through two successive steps: carbonization of biomass under N_2 flow, followed by chemical activation using KOH [6] that chemically modifies the physical structure of the biomass [7]. Therefore, waste CG-derived AC is beneficial owing to the catalytic support rendered and its cost-effectiveness, large surface area, and chemical inertness in both acidic and basic media [8].

Most metal-based reduction catalysts rely heavily on noble metals such as Au nanoparticles (NPs), PdNPs, and PtNPs [9]. PdNPs are metal NPs that are frequently used as catalysts in heterogeneous reactions because of their high catalytic activity and selectivity [10]. Although PdNPs as solid catalysts have excellent catalytic reduction performance, bare PdNPs cause easy aggregation and non-recyclability if not effectively protected or stabilized [11]. To overcome these drawbacks, bare PdNPs must be immobilized by suitable supports that enhance the effectiveness of the supported metal NPs by acting as catalytically active centers [12]. Therefore, considering economic feasibility and environmental concerns, AC derived from waste CGs can be an appropriate catalyst support. NPs are typically loaded directly onto supports or via the reduction of a metal precursor ($PdCl_2$) in the support. Direct NP deposition on a support has been used increasingly because it enables greater control over the particle size and morphology.

The catalytic reduction of 4-nitrophenol (4NP) is widely used as a model reduction reaction because of its high aqueous-phase stability. Furthermore, 4-aminophenol (4AP), the hydrogenated form of 4NP, is an important intermediate in the production of analgesic and antipyretic drugs [13]. Moreover, converting the highly toxic 4NP into the less toxic 4AP is preferred [14].

Therefore, in this study, AC derived from waste CGs was used to catalyze the reduction of 4NP to 4AP. After pyrolysis, carbonization, and activation by KOH, the waste CG was recycled as a catalyst support to improve the life span of the catalyst (PdNPs) and ensure reusability in chemical processes. Carbonized and activated CGs are referred to as CCGs and ACGs, respectively. The temperature of pyrolysis with N_2 flow to form CCG from CG was adjusted from 400 to 700 °C to optimize the carbonization temperature. Their pore properties, namely their surface areas, were investigated using N_2 adsorption/desorption isotherms. CCG activation with KOH treatment was performed sequentially at 700 °C under N_2 flow conditions. PdNPs loaded on ACGs (PdNPs@ACG) were applied as a potential catalyst for 4NP reduction, and continuous usability and reliability tests were conducted. In addition, both Pd precursor-based catalysts ($PdCl_2$@ACGs) and bare PdNPs were tested to compare their catalytic performance. Although the results of 4NP reduction using Pd-supported waste CGs are easily found in the literature [12-14], only few reports on the reusability test for PdNPs@ACG exist. Therefore, in this study, the stability and reusability of PdNPs@ACG

†To whom correspondence should be addressed.
E-mail: rengaraj@squ.edu.om, korea1@kw.ac.kr

for the catalytic reduction of 4NP were investigated for five recycling processes.

EXPERIMENTAL

1. Preparation of ACG from CG

Waste CGs, made entirely from Brazilian Specialty beans after roasting and dripping, were obtained from Paik's Cafe. To remove the brown color and any lingering organics, the CGs were washed five times with a 0.1 M NaOH solution and deionized (DI) water. The washed CGs were filtered through a sieve with a mesh size of 75 μm, and the filtered CGs were collected for use as a support. The collected CGs were dried in a vacuum oven at 120 °C for 24 h. These dry grounds were subsequently heated for 2 h at 400-700 °C under N_2 flow at a ramping rate of 10 °C/min to carbonize and remove volatile organics. A CCG at 500 °C is referred to as CCG_{500}. Following chemical activation, KOH and the CCGs were ground with a mortar and pestle to produce a fine gray mixture [15]. The weight ratio of KOH to CCG was set at 4 : 1. The mixture was subsequently introduced into a furnace for pyrolysis at 700 °C under N_2 flow, heating at 3 °C/min, and dwelling for 1 h. Finally, solid black carbon, ACG, was obtained.

2. Preparation of PdNP@ACG and $PdCl_2$@ACG

To load PdNPs on the ACG support, PdNPs were prepared by a simple reduction method adapted from the preparation of AgNPs [16]. Prior to adding 1 mL of 50 mM trisodium citrate (TSC) and 0.6 mL of 100 mM $NaBH_4$, 2 mL of 2.5 mM $PdCl_2$ and 17 mL of DI water were mixed and stirred for 10 min. The mixture was stirred vigorously for 30 min. Thereafter, 190 mg of ACG was added to 20.6 mL of the as-prepared PdNP solution and stirred for 12 h at room temperature to saturate the PdNPs on the support. The supernatant was removed after centrifugation at 11,000 rpm for 25 min. The PdNPs dispersed in the water phase that were not loaded on the support pores were removed in this step. Finally, PdNPs@ACG was obtained.

To prepare the $PdCl_2$@ACG catalyst [11], 3 mL of 56 mM $PdCl_2$ and 20 mL of 20 mM HCl were combined and heated for 30 min at 60 °C. Subsequently, 0.2 g of ACG was added to the mixture and allowed to react at 90 °C for 3 h to obtain $PdCl_2$@ACG. The unreacted Pd precursor and PdNPs unloaded on the support were removed by the same centrifugation process used to prepare the PdNPs@ACG. The loading weight of Pd on the ACG was determined via inductively coupled plasma optical emission spectrometry (ICP-OES, Avio 200, PerkinElmer). Finally, the as-prepared catalysts (PdNPs, PdNPs@ACG, and $PdCl_2$@ACG) were diluted in DI water before characterization and participation in the catalytic reaction.

3. Catalytic Reduction of 4NP

The catalytic performances of PdNPs, PdNPs@ACG, and $PdCl_2$@ACG for the reduction of 4NP with $NaBH_4$ as the reducing agent were evaluated. The 4NP solution (8 mL, 100 ppm) and $NaBH_4$ (10 mL, 0.1 M) were added to 50 mL of DI water. The solution was transferred to a round-neck bottle, and the catalyst solution (1 mL, 60 ppm for Pd-based 0.33 wt%) was added to the bottle, which was subsequently sealed with aluminum foil to prevent 4NP photolysis by sunlight [17]. UV-vis spectroscopy was performed to confirm the catalytic reduction of 4NP to 4AP. The used catalysts were centrifuged, and the supernatant was removed after the first catalytic reaction. In the reducibility test, a mixture of 4NP and $NaBH_4$ was added to the catalyst solution (1 mL), which remained after centrifugation. This procedure was repeated four times.

4. Characterization

Transmission electron microscopy (TEM, JEM-2010, Jeol) and field-emission electron microscopy were performed to examine the sample morphology (SEM, JSM-6700F, Jeol). A spectrometer (UV-1800, Shimadzu) was used to measure the UV-vis absorbance spectra. The mass change with the temperature of CG was investigated using derivative thermal gravimetry (DTG, DTG-60H, Shimadzu) through thermal gravimetric analysis (TGA). The pore properties of the samples were measured via N_2 adsorption/desorption isotherms using a Micromeritics 3Flex analyzer. The changes in the surface composition of the samples during carbonization and activation were investigated via Fourier-transform infrared spectroscopy (FT-IR, FT/IR-4600, Jasco). The X-ray diffraction (XRD) patterns of the samples were obtained using a D/MAX-2500V diffractometer (Rigaku). Inductively coupled plasma-optical emission spectrometer (ICP-OES, Avio 200, Perkin-Elmer) was used to measure the concentration of Pd leached from PdNPs@ACG and $PdCl_2$@ACG after repeated catalysis reaction.

RESULTS AND DISCUSSION

1. Characterization of ACG

Waste CGs were carbonized via pyrolysis under N_2 condition and subsequently activated with KOH treatment with CCG. The sequential processes yielded ACGs with a high surface area and open textural porosity, which are suitable for loading PdNPs onto the ACG pore surface. The textural properties of the final products were significantly influenced by the pyrolysis temperature. Therefore, TGA and DTG analyses were performed before the pyrolysis process, as shown in Fig. 1. Because CG was completely dried in a vacuum oven, a small amount of water was removed in the first region, ranging from 25 to 200 °C. Between 250-350 °C, approximately 40 wt% of the CGs was lost, indicating that lignocellulose

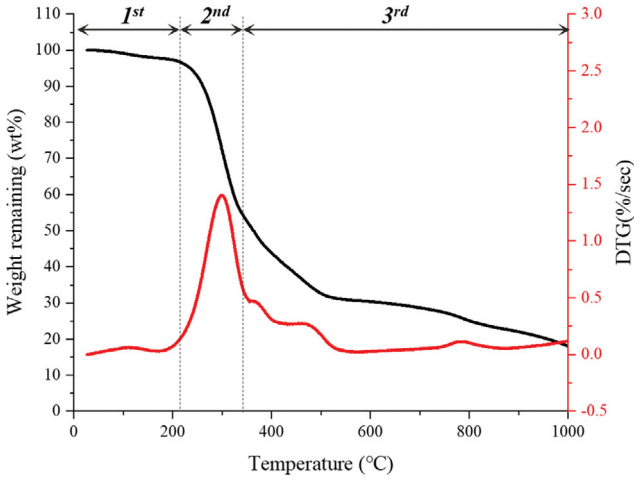

Fig. 1. TGA curve (black) and DTG curve (red) for waste CGs under N_2 conditions.

degradation had resulted in heavier hydrocarbons (tar) and gaseous products (CO, CO_2, and CH_4) [15]. Tar evolution may have occurred up to 500 °C, and the weight loss observed between 500 °C and 800 °C may be attributed to char consolidation. This feature was discovered during the formation of charcoal from CG [18]. CCG char without char consolidation was produced via thermal treatment at 500 °C. Above 500 °C in the DTG, a plateau region was reached, and the material was completely carbonized. The release of non-carbon elements in the form of gases and tars resulted in rudimentary macroporosity on the char fraction, leaving a rigid carbon skeleton formed by an irregular open textural structure [19]. Therefore, the pyrolysis temperature was increased from 400 to 700 °C, resulting in weight losses of 55.8, 70.6, 73.1, and 74.3 wt% via burn-off for CCG_{400}, CCG_{500}, CCG_{600}, and CCG_{700}, respectively.

SEM was used to examine the morphological changes caused by the sequential thermal treatment and KOH activation. As shown in Fig. 2(a), the original waste CGs were bulky, exhibiting irregular surfaces and no macropores. In contrast, sponge-like macropores were observed in the carbonized CCGs. The release of pyrolysis gases and tar may have caused this distinct textural porosity. However, certain macropores in CCG were blocked and clogged by residual carbon (Fig. 2(b)). Therefore, additional thermal or chemical treatments were required to achieve a smooth surface with a clean textural porosity.

In general, KOH and HCl are used as basic or acidic reagents for the chemical activation of carbon materials [7]. Particularly, the pyrolysis of a mixture of KOH and CCGs can result in the formation of pores in the carbon frame structure [4]. Therefore, a 4 : 1 weight ratio of KOH and CCG powder was mixed with a mortar and subsequently pyrolyzed at 700 °C. As shown in Fig. 2(c), the surface of the ACG became cleaner, and its pores widened. The chemical activation and pore formation reactions with KOH followed the reactions listed below [3,4,20].

$$2KOH \rightarrow K_2O + H_2O \quad (1)$$

$$C + H_2O \rightarrow CO + H_2 \quad (2)$$

$$6KOH + 2C \rightarrow 2K + 3H_2 + 2K_2CO_3 \quad (3)$$

$$K_2CO_3 + 2C \rightarrow 2K + 3CO \quad (4)$$

The possible reactions of KOH activation are represented by reactions (1) or (3) [20]. The pyrolysis of KOH produces H_2O or K_2CO_3 that subsequently reacts with carbon materials to form CO or H_2 at 700 °C [4]. The porous structure of an ACG is formed when

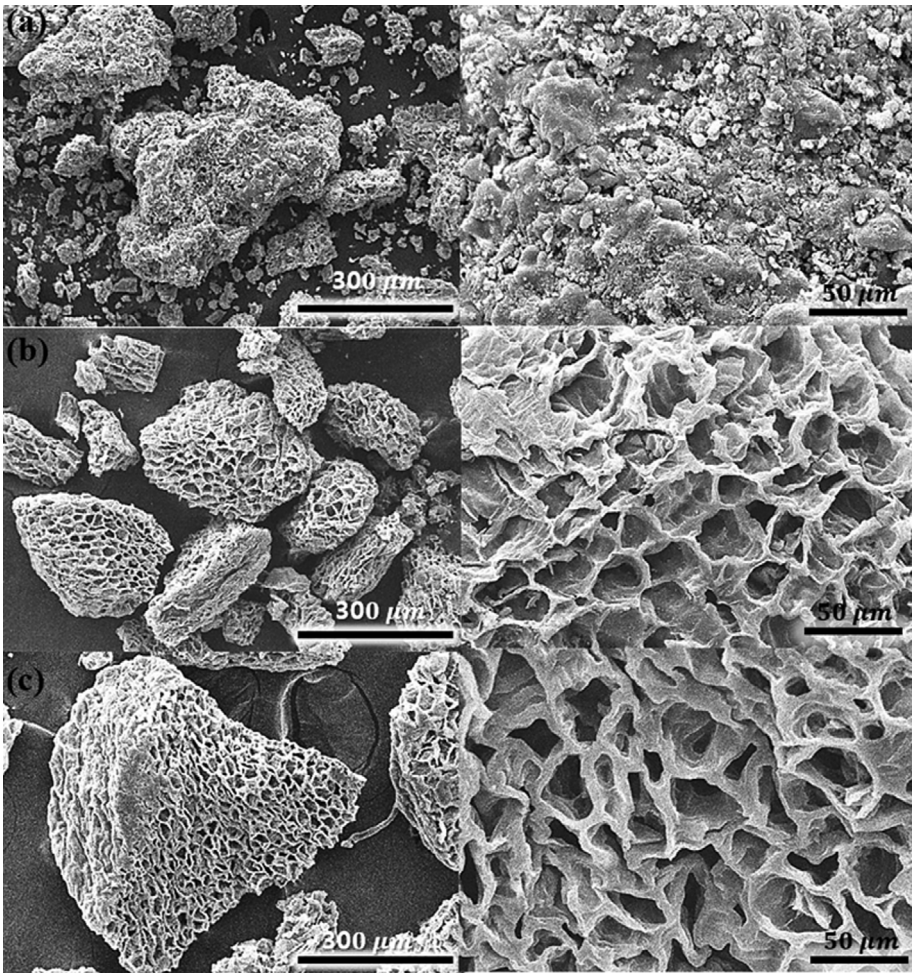

Fig. 2. SEM images of (a) CG, (b) CCG_{600}, and (c) ACG_{600} samples.

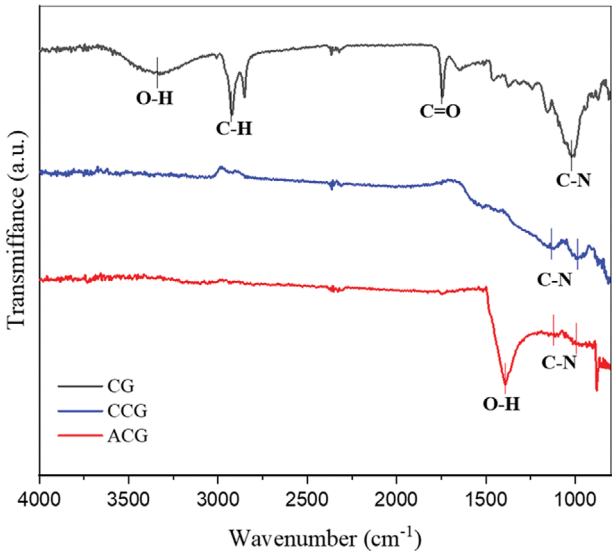

Fig. 3. FT-IR spectra of CGs, CCG_{600}, and ACG_{600}.

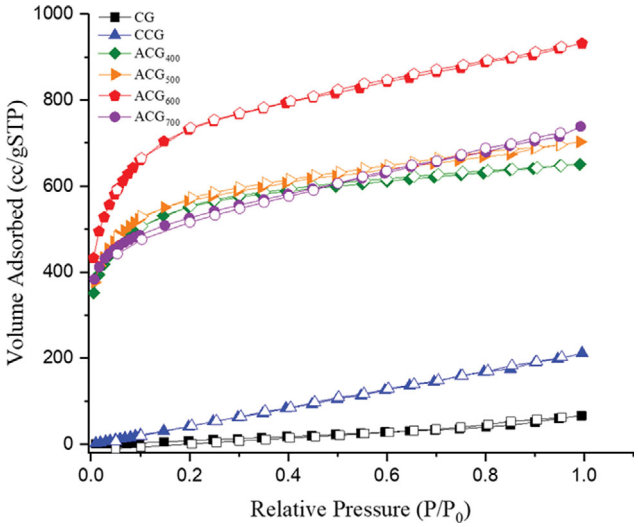

Fig. 4. N_2 adsorption/desorption isotherms of CGs, CCGs, and ACGs at various carbonization temperatures from 400 to 700 °C.

water vapor and carbon undergo steam reforming reaction (2) or when K_2CO_3 and carbon undergo redox reactions (4) [3,4]. KOH activation generally produces wormhole-like micropores (ca. 1-2 nm) in the ACG backbone, indicating the presence of amorphous porous carbon [4]. The micropores of the ACG backbone are not useful for loading PdNPs; therefore, the textural structure of ACG with macropores (15-50 μm) is of interest in this work, as shown in the magnified SEM image in Fig. 2(c). The three-dimensional structure with many holes is better suited for aqueous phase reactions, [21] and it is also favorable for the easy loading of PdNPs on the surface of the ACGs.

The catalytic reaction depends on the successful loading of PdNPs onto the ACG support. FT-IR analysis of CG, CCG, and ACG was performed to verify the functionality of the surface of the ACGs. As shown in Fig. 3, the FT-IR spectra of the three samples exhibit distinct peaks. Waste CGs exhibit a broad band at 3,400 cm^{-1} owing to the stretching vibration of O-H groups originating from water, phenols, or alcohols adsorbed onto the CGs [7]. The peaks at 2,900-3,000 cm^{-1} and 1,740 cm^{-1} may be attributed to C-H stretching (aliphatic) and C=O stretching vibrations (ketones or carboxyl groups), respectively [19]. The C-N stretch sample typically appears in the region of 1,250-1,020 cm^{-1} in the IR spectrum of CCs. During heat treatment and pretreatment of coffee, the C-N peak gradually weakens, which is likely due to the breakdown of these organic compounds. After carbonization, the characteristic peaks of O-H, C-H, and C=O stretching in the CCGs were eliminated. After KOH activation and additional pyrolysis, the ACGs reveal new peaks at 1,320-1,400 cm^{-1}, indicating the O-H bending modes of alcoholic or carboxylic groups [6]. The hydroxyl groups with an actual peak at 1,370 cm^{-1} can be used to bind the PdNPs on the ACG support.

The large surface area of the support is an important property in catalytic reactions because it allows more reactants to reach the catalytic sites. To analyze the surface area and pore volume of the as-prepared samples, N_2 adsorption/desorption isotherms were measured (Fig. 4). The pore properties of the catalysts are summarized in Table 1. Both the CGs and CCGs exhibit typical type-III isotherms, according to the IUPAC classification [19], which are obtained when the formation of monolayers, bilayers, and other layers occur simultaneously, resulting in an almost linearly increase in the amount of adsorption. They exhibit no micropores; thus, their surface areas are small: 259 and 374 m^2/g for the CGs and CCGs, respectively. Although the macropores in the CCGs were fully developed in comparison to the CGs, the CCGs prior to KOH

Table 1. Pore properties of CGs, CCGs, and ACGs at the carbonization temperature

Samples	Temperature conditions		Pore properties		
	Carbonization (°C)	Activation (°C)	Surface area (m^2/g)	Micropore size (nm)[a]	Pore volume (cm^3/g)
CGs	-	-	259.1	-	0.254
CCG_{500}	500	-	374.4	-	0.306
ACG_{400}	400	700	2,016.5	3.1	0.156
ACG_{500}	500	700	2,144.6	1.5	0.226
ACG_{600}	600	700	2,710.3	1.9	0.312
ACG_{700}	700	700	1,948.3	3.0	0.407

[a]Micropore size was determined from the desorption average pore diameter (4 V/S).

activation treatment lacked micropores and exhibited a small surface area. After sequential carbonization and KOH activation, the ACGs exhibited a type-I isotherm with a large surface area. The steep increase in the adsorption curve at low relative pressures indicates the development of narrow microporosity [15]. Because of the small hysteresis and deviation from the plateau region in the isotherm plots, ACGs exhibit few mesopores [7]. The KOH activation process clearly influenced the surface area of the ACG support. The surface area of ACG_{500} after activation is 5.7 times greater than that of CCG_{500}. As described earlier, the reactions for chemical activation and pore formation with KOH were induced such that the surface of the ACG became clean and its pores widened. In addition, the surface area of the support was affected by carbonization temperature. As shown in Table 1, ACG_{600} exhibits a large surface area and pore volume and well-developed microporosity and macroporosity. Therefore, in this study, ACG_{600} was chosen as a support for loading PdNPs.

2. Characterization of PdNPs@ACG

Herein, citrate-stabilized PdNPs were prepared using a simple reduction method with a Pd precursor and subsequently loaded onto an ACG support via hydroxyl group binding. The prepared catalyst was referred to as PdNPs@ACG. Another catalyst, $PdCl_2$@ACG, was prepared via the in situ reduction of Pd ions under acidic conditions. Because no additional reducing agent is used in the preparation of $PdCl_2$@ACG, the hydroxyl groups present in the ACGs formed by pyrolysis and KOH activation can gradually reduce the Pd(II) metal ion to a zero-valent state under HCl conditions [11, 22]. The hydroxyl groups found in the biomass-based supports acted as reducing agents, whereas other groups containing O acted as stabilizers during the formation of PdNPs [23]. This in situ reduction of Pd ions to PdNPs is considered a green synthesis approach [22,23]. Because the carbon backbone of ACGs is composed of micropores, in situ reduced Pd in $PdCl_2$@ACG could be loaded on both the micropores and macropores of the ACGs. In contrast, citrate-stabilized PdNPs in the PdNPs@ACG were generally loaded on the macropores and outer surface of the ACG support.

XRD analysis was performed to verify the loading of PdNPs on the ACGs (Fig. 5). Planar graphite (002) and (101) that correspond

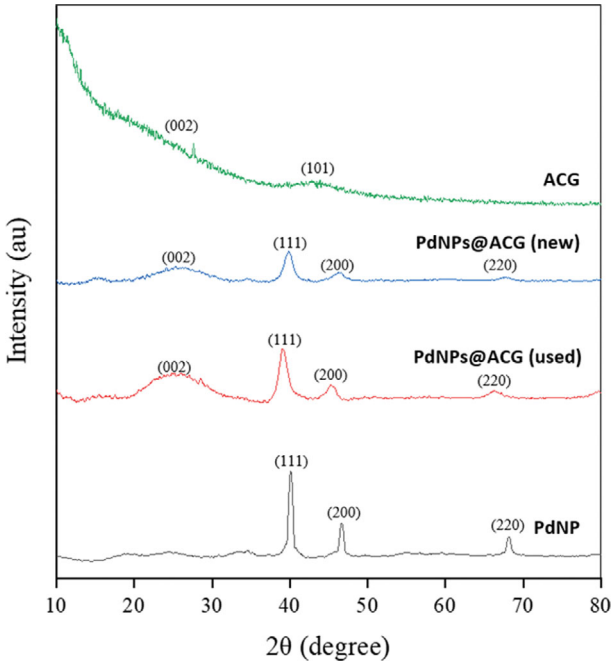

Fig. 5. XRD patterns of ACGs, PdNPs@ACG (new), PdNPs@ACG (used), and PdNPs.

to two broad peaks in the ACGs at approximately 23° and 43°, respectively, are similar to the graphitic hexagonal structure of carbon-based materials [24]. Apart from the carbon peak, the four characteristic peaks of the (111), (200), and (220) planes of Pd metal are visible after loading PdNPs on the ACGs, indicating the presence of metallic PdNPs on the ACGs [11]. Compared with that indicated by the XRD pattern of PdNPs, a relatively low loading of PdNPs on the ACGs is indicated by the weak Pd diffraction peaks of the samples (PdNPs@ACG).

According to the N_2 isotherm analysis, the carbon backbone of the ACGs exhibits micropores that are activated by KOH [3], which enables the in situ formation of PdNPs blocked on the micropores of the carbon backbone. The loading of the as-prepared PdNPs

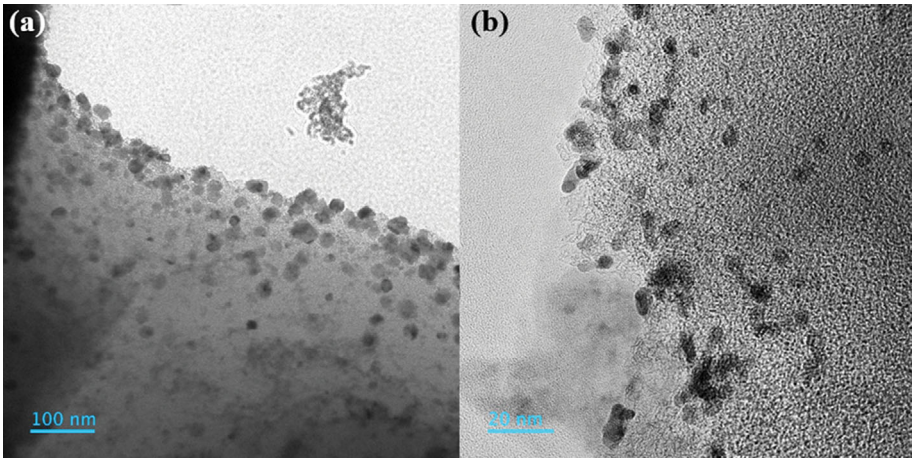

Fig. 6. TEM images of (a) PdNPs@ACG and (b) $PdCl_2$@ACG catalysts.

on the ACG is expected to occur primarily in the macropores and outer surface of the ACG. To determine the features of PdNP loading on the ACGs, TEM analysis was performed (Fig. 6). As shown in Fig. 6(a), PdNPs were effectively dispersed in the PdNPs@ACG, with an average particle size of 12.7 nm. The as-prepared PdNPs were successfully immobilized on the outer surface and macropores of the ACGs [11]. In contrast, in situ reduced Pd particles were immobilized on partial micropores and mainly on the outer surface of the ACGs [25]. The particle size of the PdNPs in the $PdCl_2$@ACG was slightly smaller than that in the PdNPs@ACG (Fig. 6(b)). PdNPs loaded in the $PdCl_2$@ACG exhibited an average size of 5.2 nm. Consequently, the loading of the PdNPs depended on the preparation method of the catalyst. Thus, the catalytic activity might also vary with the type of catalyst.

3. Catalytic Reduction of 4NP Using PdNPs@ACG

The catalytic activity of the PdNPs@ACG was examined by the reduction of 4NP to 4AP in the presence of $NaBH_4$. The absorption peak of the 4NP solution red-shifted from 317 nm (light yellow) to 400 nm (deep yellow) immediately after the addition of $NaBH_4$ owing to the formation of 4NP ions [17]. Therefore, the catalytic performance was quantified via UV-vis spectroscopy. As a blank test, the catalytic reduction of 4NP using ACG was investigated, and Fig. 7(a) shows the UV-vis spectra of 4NP as a function of reaction time. No change in the absorbance was observed, and no new peak corresponding to 4AP was observed. Although the catalytic reduction of 4NP in the presence of $NaBH_4$ is thermodynamically favorable, it is kinetically restricted because of the higher reduction potential of 4NP to 4AP [26]. This indicates that ACG does not adsorb 4NP and is not catalytically active on its own. The intensity of the strong absorbance peak at 400 nm was considerably reduced by the catalytic reduction of 4NP ions by $NaBH_4$, catalyzed by PdNPs dispersed in the solution, and a new peak for 4AP at 300 nm was immediately observed (Fig. 7(b)). The reduction conversion of 4NP using PdNPs reached 97% within 90 s. In the case of catalytic reduction using the PdNPs@ACG, the main peak for 4NP gradually decreased, and a 4AP peak appeared at 300 nm; 630 s was required for 97% conversion of 4NP (Fig. 7(c)). The catalytic reduction using the $PdCl_2$@ACG was completed in 450 s with 97% reduction conversion (Fig. 7(d)).

Generally, as the reduction of 4NP to 4AP progresses, the intensity of the characteristic peaks of 4AP increases [17,27]. However, certain inconsistencies were observed in the UV-vis signal at 300 nm, and thus, its intensity did not increase consistently or proportionally, as would have been expected. In this study, as the reaction progressed, the intensity of the peak of 4AP at 300 nm decreased (Fig. 7(c)), a feature that has also been reported in other studies [27-30]. The decrease in the signal intensity at 300 nm, associated with the presence of O_2 gas in the solution, indicates consumption of 4AP [31]. One possible catalytic mechanism involves the adsorption of $4NP^-$ onto the catalyst surface, followed by its reduction to 4AP by hydrogen derived from BH_4^- under alkaline conditions. Once produced, 4AP is rapidly desorbed from the surface

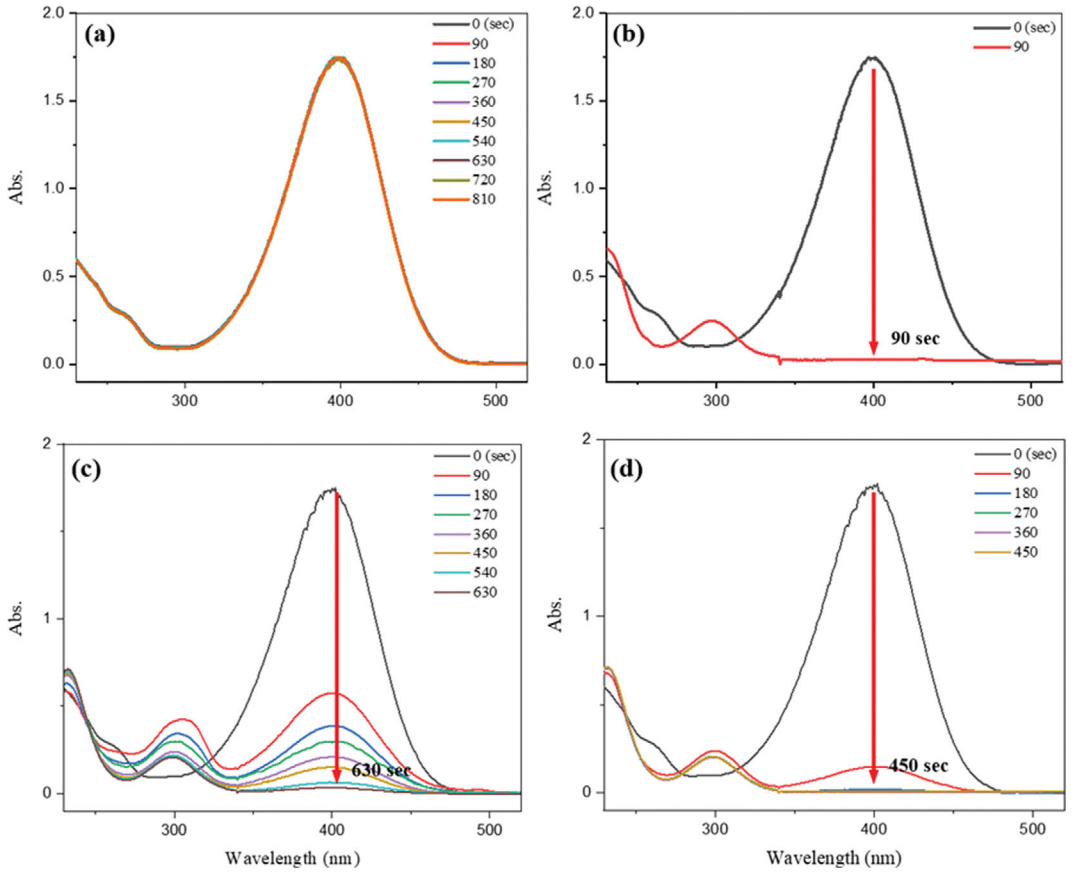

Fig. 7. UV-vis spectra for the catalytic reduction of 4NP using (a) ACG_{700}, (b) PdNPs, (c) PdNPs@ACG, and (d) $PdCl_2$@ACG.

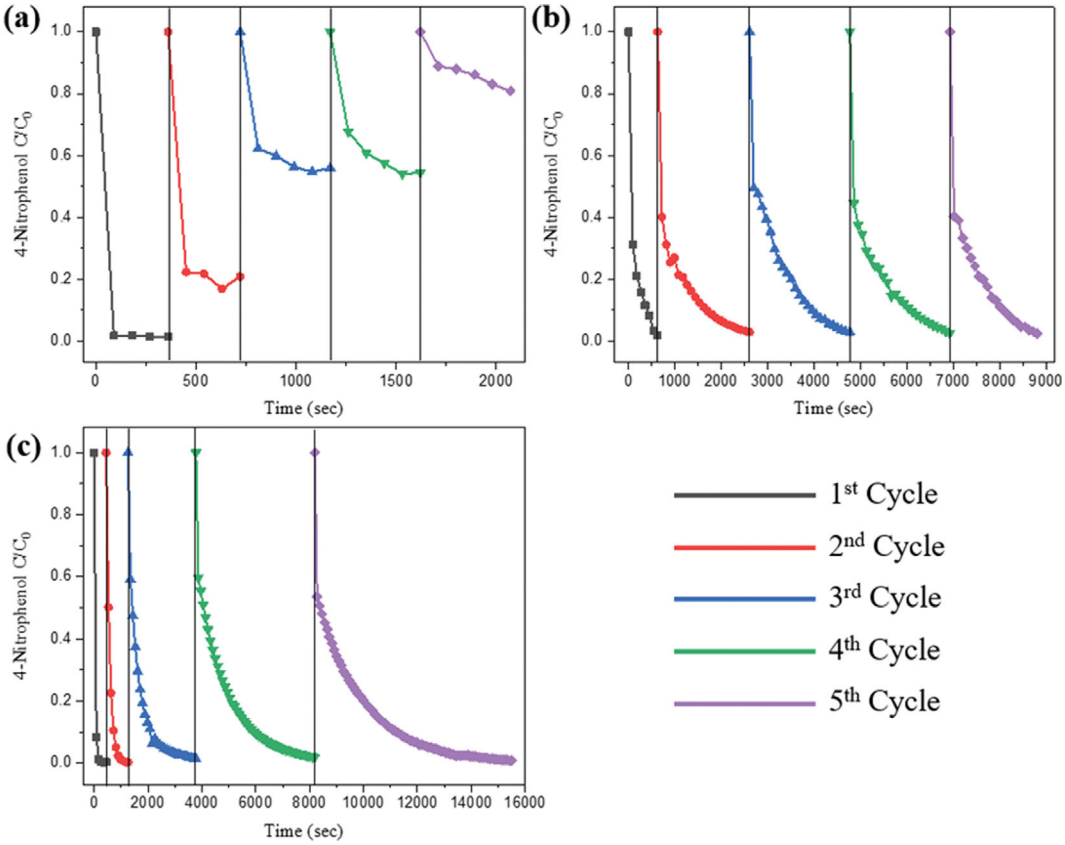

Fig. 8. Repeated catalytic reduction of 4NP using (a) PdNPs, (b) PdNPS@ACG, and (c) $PdCl_2$@ACG for five cycles.

[32]. At this stage, instead of converting $4AP^-$ to $4NP^-$, $4AP^-$ can be lost through conversion to other oxidized species [27]. Because aqueous 4AP can decompose into quinone derivatives [33], hydroquinone and benzoquinone derivatives produced by the additional oxidization of $4AP^-$ can be detected in the UV-vis spectra. The two spectra are in the 220-300 nm range (Fig. 7(c)), but the production of quinones could not be determined because the two spectral regions of 4AP overlapped with those of quinones [27]. Therefore, calculation of the reduction conversion of 4NP with intensity change for 4NP at 400 nm rather than the 4AP peaks at 220-300 nm was preferred.

According to the results shown in Fig. 7, PdNPs dispersed in solution appear to be the most effective catalyst when compared with the ACG-supported Pd catalysts. However, if suitably protected or stabilized, bare PdNPs dispersed in the aqueous phase easily aggregate and become non-recyclable [11]. Therefore, conducting a reusability test is necessary. The performance of repeated catalytic reduction using the PdNPs, PdNPs@ACG, and $PdCl_2$@ACG over five reaction cycles is shown in Fig. 8. Pseudo-first-order kinetics governs the reduction reaction of 4NP [26], and Table 2 presents the reaction rate for five cycles. The reduction conversion of PdNPs without support was considerably reduced from the second cycle (82%) to fifth cycle (20%), as shown in Fig. 8(a). PdNPs dispersed in the aqueous phase could be easily aggregated and partially removed during the recycling step [9], resulting in a lower reduction conversion. After conducting TEM analysis of the $PdCl_2$@ACG catalyst following repeated experiments, it was observed that the amount of PdNP fixed on the support was significantly less than that shown in Fig. 6(b). This indicates that there is leaching of these catalytic sites, which could be impeding the catalytic reaction performance. In addition, the reaction rate (min^{-1}) of PdNPs decreased from 0.27 to 0.02. In contrast, the reduction conversion of PdNPs with the support (PdNPs@ACG and $PdCl_2$@ACG) was maintained above 97% for five cycles (Fig. 8(b) and 8(c)). Until the second cycle, the completion time and reaction rate of the $PdCl_2$@ACG were better than those of the PdNPs@ACG. However, the reaction rate of $PdCl_2$@ACG decreased gradually from 0.72 to 0.04. In the preparation step, certain Pd precursors ($PdCl_2$) could enter the micropores of the ACGs and form PdNPs on the carbon backbone. Therefore, the catalytic activity decreased owing to micropore blockage and loss of PdNPs during repeated catalytic reactions and regeneration. However, the PdNPs@ACG maintained

Table 2. Rate constant change of 4NP reduction using PdNPs, PdNPs@ACG, and $PdCl_2$@ACG during five cycles

Samples	Rate constant (min^{-1})				
	k_1	k_2	k_3	k_4	k_5
PdNPs	0.27	0.23	0.07	0.07	0.02
PdNPs@ACG	0.34	0.08	0.09	0.08	0.10
$PdCl_2$@ACG	0.72	0.45	0.09	0.05	0.04

Table 3. Comparison of reaction rate of different catalytic systems for the 4NP reduction

Support	Catalyst	Reaction rate (min^{-1})	Recycle test	References
Waste coffee	Pd	0.10-0.34	5 cycles	This work
Activated carbon	Au	0.07-0.25	5 cycles	[34]
Waste coffee	Ag	0.01-0.27	7 cycles	[35]
Waste coffee	Au	0.28	4 cycles	[36]
Gold crystal	Carbon dot	0.11-0.30	-	[37]
Activated carbon	Au	0.53	-	[38]
Graphene oxide	Ag	0.25-0.37	5 cycles	[39]

adequate stability over five cycles (Fig. 8(c)), and its reaction rate after the second cycle was 0.08-0.10 min^{-1}. To confirm the stability of the catalyst, XRD and ICP analysis was performed on samples recovered after repeated experiments. In the case of the PdNP and $PdCl_2$@ACG catalysts, the activity of the catalyst decreased due to the separation of Pd particles. The ICP analysis revealed that Pd was eluted up to 16.6 ppm after repeated experiments in the $PdCl_2$@ ACG catalyst, which initially contained 60 ppm Pd. Namely, after the first and second experiments, the amount of leached Pd was less than 10% (2.5 and 5.2 ppm for the first and second test, respectively) of the initial concentration. While, after the fifth experiment, the leaching amount corresponded to 27% of the initial Pd concentration. This indicates that some large-particle PdNPs were leached out of the catalyst during the repeated cycles, and this phenomenon was correlated with the observed decrease in performance after the second cycle. The PdNP catalyst exhibited a decrease in catalytic activity due to a loss in the amount of catalyst during the sample recovery process. This performance degradation due to the detachment of metal nanoparticles was also observed in Au/C catalysts used in the 4NP reduction reaction [34]. On the other hand, the PdNPs@ACG catalyst experienced only a slight decrease in Pd content, with 6.5 ppm of Pd being detected after one experiment. However, the catalytic performance was maintained thereafter. Namely, the PdNP@ACG catalyst experienced a leaching of only 10% after the first experiment, but no further leaching occurred subsequently.

This suggests that the PdNPs@ACG catalyst demonstrated better stability compared to the PdNP catalyst. Furthermore, the XRD results (shown in Fig. 5) indicate that the crystal phase of the catalyst was maintained even after repeated use. It is noted that the catalyst particles that were excessively attached to the outside of the reactor came off, but the performance of the catalyst remained stable after this point. These results suggest that while some loss of the catalyst occurred over multiple cycles of use, the catalyst remained effective in promoting the reduction of 4NP to 4AP. However, further studies may be necessary to investigate the long-term stability and durability of the catalyst.

Additional catalytic reactions were carried out at 20, 40, and 60 °C to determine the activation energy, which was calculated to be 92.54 J/mol. In another study where gold nanoparticles were immobilized on activated carbon, the rate constant was observed to be between 0.07-0.25 min^{-1} with an activation energy of 26.38 kJ/mol [35]. Table 3 is organized for comparison of the catalytic performance of other carbon-based materials. When waste coffee was used, the rate was generally observed to be 0.30 min^{-1}, and with repeated cycles most of the catalytic performance decreased rapidly [36]. However, in this study, the performance was maintained from the second cycle. Graphene oxide showed the highest performance, while activated carbon also demonstrated excellent 4NP reduction ability depending on conditions [37-39]. In terms of reusing wasted organic carbon, the use of catalysts using waste coffee is considered more environmentally friendly. Therefore, the initial reaction rate of the catalytic reduction of 4NP using PdNPs@ACG may not be high; however, PdNPs@ACG is an effective and environmentally friendly catalyst for continuous use.

CONCLUSIONS

An environmentally friendly catalytic support containing PdNPs was prepared for the catalytic reduction of 4NP. Two types of catalysts were prepared using traditional methods: loading of PdNPs on the support and in situ reduction of Pd ions to PdNPs on the support. Sequential pyrolysis and KOH activation at various temperatures were applied to achieve porosity and activate the surface of CGs, and an ACG support was obtained through carbonization at 600 °C and activation at 700 °C. ACGs exhibited a larger surface area (2,710 m^2/g) than CCGs (374 m^2/g) because of the development of micropores on the carbon backbone of the ACGs. In addition, ACG macropores were suitably developed to immobilize the as-prepared PdNPs without pore blocking. In the first cycle of the catalytic reduction of 4NP, PdNPs dispersed in the aqueous phase without support exhibited a high reaction rate and good conversion efficiency. However, after repeated recycling of the catalyst, the catalytic performance of PdNPs was considerably reduced owing to the aggregation of PdNPs and loss of catalyst during the recycling process. In contrast, the PdNP catalyst supported by ACGs demonstrated long-term stability over five recycling processes. In particular, compared with $PdCl_2$@ACG after three cycles, the PdNPs@ACG exhibited a stable and uniform reaction rate with high conversion. Consequently, carbonized and KOH-activated ACGs can be used as a potential support owing to their adequate stability and environmental friendliness.

ACKNOWLEDGEMENTS

This work was conducted with research funds of the Research Grant of Kwangwoon University (2023) and the National Research Foundation of Korea (NRF-2022R1F1A1059495).

REFERENCES

1. P. Esquivel and V. M. Jiménez, *Food Res. Inter.*, **46**, 488 (2012).
2. B.-S. Baek, J.-W. Park, B.-H. Lee and H.-J. Kim, *Polym. Environ.*, **21**, 702 (2013).
3. M.-J. Kim, S. W. Choi, H. Kim, S. Mun and K. B. Lee, *Chem. Eng. J.*, **397**, 125404 (2020).
4. C.-H. Wang, W.-C. Wen, H.-C. Hsu and B.-Y. Yao, *Adv. Powder Technol.*, **27**, 1387 (2016).
5. J. Roh, H. N. Umh, C. M. Yoo, S. Rengaraj, B. Lee and Y. Kim, *Korean J. Chem. Eng.*, **29**, 903 (2012).
6. E. Pagalan Jr, M. Sebron, S. Gomez, S. J. Salva, R. Ampusta, A. J. Macarayo, C. Joyno, A. Ido and R. Arazo, *Ind. Crops Prod.*, **145**, 111953 (2020).
7. H. Laksaci, A. Khelifi, B. Belhamdi and M. Trari, *J. Environ. Chem. Eng.*, **5**, 5061 (2017).
8. M. Gurrath, T. Kuretzky, H. P. Boehm, L. B. Okhlopkova, A. S. Lisitsyn and V. A. Likholobov, *Carbon*, **38**, 1241 (2000).
9. H. Hu, J. H. Xin, H. Hu, X. Wang, D. Miao and Y. Liu, *J. Mater. Chem. A*, **3**, 11157 (2015).
10. K. Karaoglu, Z. Özçifçi, M. Çaliskan, T. Baran and H. T. Akçay, *Mater. Chem. Phys.*, **282**, 125857 (2022).
11. H. Chan, C. Shi, Z. Wu, S. Sun, S. Zhang, Z. Yu, M. He, G. Chen, X. Wan and J. Tian, *J. Colloid Interface Sci.*, **608**, 1414 (2022).
12. P. S. Shinde, P. S. Suryawanshi, K. K. Patil, V. M. Belekar, S. A. Sankpal, S. D. Delekar and S. A. Jadhav, *J. Compos. Sci.*, **5**, 75 (2021).
13. M. J. Vaidya, S. M. Kulkarni and R. V. Chaudhari, *Org. Process Res. Dev.*, **7**, 202 (2003).
14. M. Kang and Y. Kim, *J. Ind. Eng. Chem.*, **86**, 61 (2020).
15. W. Travis, S. Gadipelli and Z. Guo, *RCS Adv.*, **5**, 29558 (2015).
16. M. Rozalen, M. Sánchez-Polo, M. Fernández-Perales, T. J. Widmann and J. Rivera-Utrilla, *RSC Adv.*, **10**, 10646 (2020).
17. H. Moon and Y. Kim, *ACS Appl. Polym. Mater.*, **3**, 2768 (2021).
18. A. S. González, M. G. Plaza, J. J. Pis, F. Rubiera and C. Pevida, *Energy Procedia*, **37**, 134 (2013).
19. H. Laksaci, A. Khelifi, M. Trari and A. Addoun, *J. Clean. Prod.*, **147**, 254 (2017).
20. E. Raymundo-Pinero, P. Azais, T. Cacciaguerra, D. Cazorla-Amoros, A. Linares-Solano and F. Beguin, *Carbon*, **43**, 786 (2005).
21. C.-F. Wang, C.-L. Wu, S.-W. Kuo, W.-S. Hung, K.-J. Lee, H.-C. Tsai, C.-J. Chang and J.-Y. Lai, *Sci. Rep.*, **10**, 12769 (2020).
22. O. Piermatt, *Catalysts*, **11**, 1258 (2021).
23. Z. Wang and X. Bai, *J. Mol. Struct.*, **1219**, 128538 (2020).
24. S. Sonal, P. Prakash, B. K. Mishra, G. C. Nayak, *RSC. Adv.*, **10**, 13783 (2020).
25. T. Gong, L. Qin, W. Zhang, H. Wan, J. Lu and H. Feng, *J. Phys. Chem. C*, **119**, 11544 (2015).
26. M. U. Trivedi, C. K. Patlolla, N. M. Misra and M. K. Pandey, *Catal. Lett.*, **149**, 2355 (2019).
27. J. Strachan, C. Barnett, A. F. Masters and T. Maschmeyer, *ACS Catal.*, **10**, 5516 (2020).
28. M. A. Hussain, M. Yang, T. J. Lee, J. W. Kim and B. G. Choi, *J. Colloid Interface Sci.*, **451**, 216 (2015).
29. T. K. Das, S. Ganguly, P. Bhawal, S. Mondal and N. C. Das, *Res. Chem. Intermed.*, **44**, 1189 (2018).
30. L. Lin, Y. Wen, L. Li, Y. Tan, P. Yang, Y. Liang, Y. Xu, H. Hu and Y. Xu, *Nanomaterials*, **12**, 3339 (2022).
31. E. Menumerov, R. A. Hughes and S. Neretina, *Nano Lett.*, **16**, 7791 (2016).
32. R. D. Neal, Y. Inoue, R. A. Hughes and S. Neretina, *J. Phys. Chem. C*, **123**, 12894 (2019).
33. J. Ahmed, R. H. Rakib, M. M. Rahman, A. M. Asiri, I. A. Siddiquey, S. S. Islam and M. A. Hasnat, *ChemPlusChem*, **84**, 175 (2019).
34. M. Ruan, P. Song, J. Liu, E. Li and W. Xu, *J. Phys. Chem. C*, **121**, 25882 (2017).
35. A. Kumar, M. Belwal, R. R. Maurya, V. Mohan and V. Vishwanathan, *Mater. Sci. Energy Technol.*, **2**, 526 (2019).
36. R. P. Lopes, T. Guimarães and D. Astruc, *J. Braz. Chem. Soc.*, **32**, 1680 (2021).
37. Y. Zhu, J. Du, Q. Peng, F. Wang, J. Hu, Y. Luo, A. A. Alshehri, K. A. Alzahrani, B. Zheng, X. Sun and D. Xiao, *RSC Adv.*, **10**, 19419 (2020).
38. H. R. Molina, J. L. S. Muñoz, M. I. D. Leal, T. R. Reina, S. Ivanova, M. Á. C. Gallego and J. A. Odriozola, *Front. Chem.*, **7**, 548 (2019).
39. Z. Mohammadi and M. H. Entezari, *Ultrason Sonochem.*, **44**, 1 (2018).